Planetary Backup Bearings for Flywheel Applications

Lukas Quurck [a], Raine Viitala [b], Daniel Franz [a], Stephan Rinderknecht [a]

[a] Institute for Mechatronic Systems in Mechanical Engineering (IMS), Technical University Darmstadt
Otto-Berndt-Straße 2, 64287 Darmstadt, Germany, quurck@ims.tu-darmstadt.de
[b] Aalto University School of Engineering, Department of Mechanical Engineering
Sähkömiehentie 4P, P.O. Box 14400, 00076 AALTO, Finland, raine.viitala@aalto.fi

***Abstract*—High-speed flywheels can be used as kinetic energy storages for electrical energy. To increase the energy density of the flywheel, an outer rotor type flywheel can be utilized. The flywheels are supported by magnetic bearings and operated in vacuum conditions to provide a high efficiency. Backup bearings are needed to support the rotor in case of a malfunction of the magnetic bearings. However, since conventional backup bearings are not available for the high surface velocities above 200 m/s of the outer rotor type flywheels, a planetary backup bearing design was introduced.**

The present study investigates the experimental results of two test series conducted with a planetary backup bearing test rig. The rotor having similar properties to the outer rotor type flywheel was consecutively delevitated at rotational speeds of 1 – 20 krpm. In order to assess the severity of the delevitation events position, rotational speed, force, and thermal data were evaluated. The advancing wear of the planetary backup bearing was assessed with multiple methods. During the first test series, the rotor was mostly relevitated a few seconds after the drop-down. The second test series consisted only of full run-downs and led to a bearing failure.

The results suggest that the planetary backup bearing is feasible in the proposed application. Multiple full run-downs were possible with neither unwanted rotor-stator contact nor damage to the rotor, magnetic bearings or electric machine. The proposed indicators were found to be applicable in the planetary backup bearing life-time assessment. The future work includes the experimental investigation of the planetary backup bearing in a full-scale outer rotor type kinetic energy storage.

I. Introduction

A. Backup bearings for kinetic energy storages

High-speed flywheels are used as kinetic energy storages (KES) for electrical energy. Due to magnetic bearings and a vacuum environment, they have low self-discharge losses and can provide a high round-trip efficiency. Especially in high performance applications with multiple power requests each hour, they can outperform electrochemical storage technologies by having lower losses and longer lifetime [1 - 3]. Typical applications for flywheels can be found in rail or crane systems for recuperation as well as in grid services such as renewable integration or frequency regulation [4]. Because of their reliability and non-existing cyclic or calendrical ageing, flywheels are also used in uninterruptible power supplies (UPS) [5].

To ensure a high reliability and a low need of maintenance, the components and control of the magnetic bearing need to be robust against external influences or malfunctions. Because perfect reliability can never be provided, the magnetic bearings need mechanical backup bearings (BB) to prevent undesired rotor-stator contact in case of unintended rotor delevitation, which could lead to a fatal system failure. The BBs used in flywheels are highly exposed to mechanical and thermal loads and need to withstand at least one full run-down in case of a possible failure, power loss or overload of the magnetic bearings. Because of the high inertia of the flywheels, a full run-down supported by the BBs can take multiple minutes, even if electrical emergency braking is performed [6]. Due to a vacuum environment, in which most flywheels are operated, lubrication and heat transfer of the BBs are complicated. Since the rotor axis is oriented vertically in many kinetic energy storages, no strong forces, such as gravity, are exerted on the rotor in any radial direction. Thus, the vertically oriented flywheels tend to develop a continuous whirling motion. The whirling motion is induced by the contact forces between the rotor and the BB. Especially, the high friction moment of the bearings can lead to high circumferential acceleration. If the whirling frequency cannot be limited, for example by additional compliant BB supports [6], radial bearing forces can reach destructive levels and lead to a fatal system failure.

B. Outer rotor type flywheels

Outer rotor type (ORT) flywheels utilizing hollow cylinder rotors are considered in [7]. The design objective of this special rotor type was to increase the energy density of a rigid rotor, which is easily controllable with active magnetic bearings (AMB). Due to the hollow design and the utilized fibre reinforced plastic (FRP) with a high specific strength and stiffness, the bending eigenfrequencies are substantially above the rotational frequencies.

The rotor design is characterized by an inner diameter of 290 mm and a maximum speed above 15 krpm which leads to a surface velocity of 230 m/s at the BB contact zone. The maximum surface velocity at the outer circumference is above 330 m/s. Because a conventional rolling element bearing is neither available, nor easily integrable in the ORT design, a special BB design approach needs to be considered. The need for special BB approaches was introduced in [8] and [9], leading to a planetary BB design.

C. Planetary backup bearing design

The planetary backup bearing (PBB) design consists of multiple independent rollers in each plane. The design was derived from the idea of [10] without using the clearance elimination mechanism. A similar design was introduced by [11] as well. The rollers limit the radial movement of the rotor, forming a

polygon shaped orbit. This shape and the specific radial resilience help to prevent the continuous whirling motion with high frequencies and loads. Furthermore, the design shows the ability to keep the rotor in stable positions in the corners of the polygon, even if no strong external force, such as gravity is present. The resulting smooth and low speed rotor movement leads to low bearing loads and prevents rotor damages.

The presented PBB design uses comparably small rolling element bearings to support the rollers. The planetary BB meets very well the requirements of a flywheel BB. Especially, for high-speed rotors with large diameters, the planetary design provides lower inertia, faster synchronization times (acceleration to full speed during rotor contact) and lower friction compared to conventional BBs. The rotation frequency of the backup bearing rollers is much higher than the frequency of the rotor, according to the different diameters. This needs to be considered in the bearing selection, especially concerning the intense acceleration during the synchronization.

II. METHODS

A. *Test rig*

For experimental measurements, a 19 kg steel rotor (see Table 1 and Figure 1) with a gyroscopic eigenbehavior and high bending eigenfrequencies was built. Although the rotor is an inner rotor type (IRT), its characteristics mimic the ORT-flywheel. To investigate the friction and wear, the surface velocity of the BBs in the IRT-design equals the surface velocities of the BBs of the ORT-flywheel. This is achieved by steel discs of a large diameter, which partially provide the required inertia as well.

Table 1. Geometrical details of the rotor

Geometrical details	**mm**
Rotor length l_R	353
AMB distance l_{AMB}	229
BB distance l_{BB}	135
AMB length $l_{FE,AMB}$	48
Electric motor length $l_{FE,M}$	50
Diameter BB $\emptyset_{BB}$	220
Diameter electric motor $\emptyset_M$	85
Diameter AMB $\emptyset_{AMB}$	47

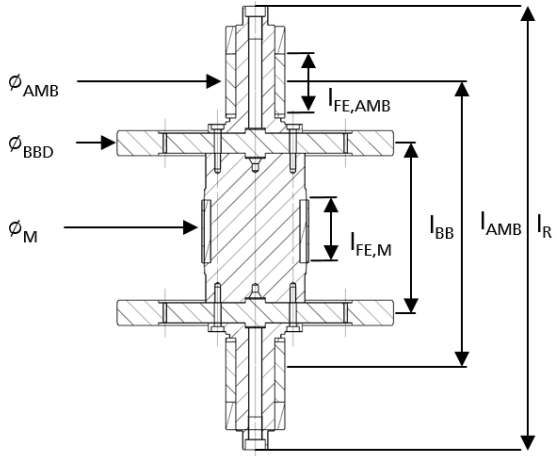

Figure 1. Schematic of the rotor.

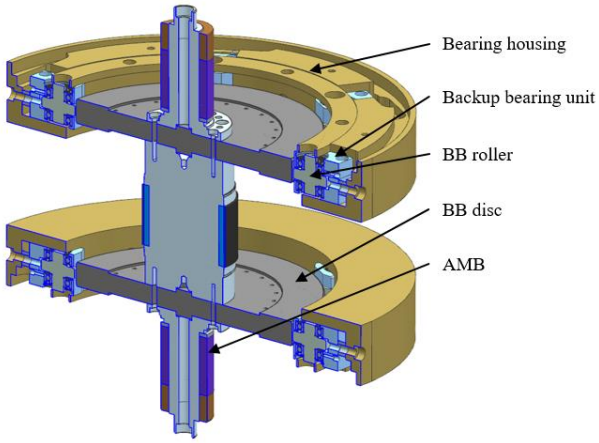

Figure 2. The rotor and the planetary backup bearings.

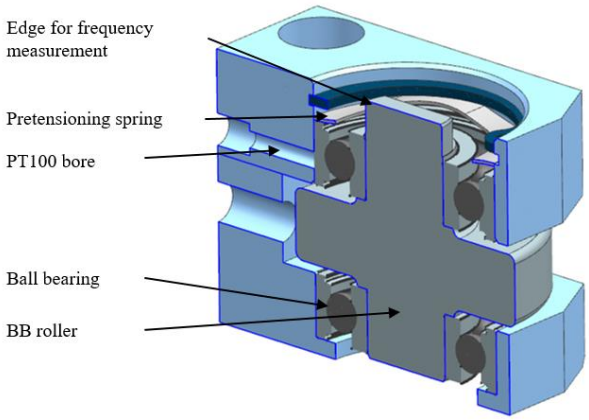

Figure 3. The backup bearing unit (BBU) consisting of two ball bearings sustaining a roller, which limits the rotor movement.

Figure 2 presents the design of the planetary backup bearing test rig. The rotor was equipped with two hardened steel discs, which were utilized as the backup bearing interface of the rotor. The test rig contained two PBBs, each of which including six backup bearing units (Figure 3) equally distributed in the backup bearing plane. The backup bearing units (BBU) consisted of a steel roller supported by two ball bearings.

The rotor was operated in a vacuum environment (circa 10^{-4} mbar) in order to maintain representative testing conditions, and delevitated at speeds from 1 krpm to 20 krpm. The maximum surface velocity in the BB plane was 230 m/s. To prevent cage failures and in order to provide high robustness in evacuated conditions, cageless hybrid spindle bearings (manufactured by GMN) were used. The bearings were angular contact ball bearings with a static load value of 2100 N. Initially they were pretensioned with circa 100 N. In the second test series, all the BBU components and the rotor discs for the BB interface were replaced. In addition, the pretension of the bearings was reduced to circa 20 N and the lubricant was changed from MoS_2 to a special vacuum grease (Krytox AB240) in order to reduce friction and provide longer bearing lifetime.

The test rig was equipped with eddy current position sensors (Eddylab T2) to measure the radial position of the rotor. In the axial direction, the position was measured by inductive Balluff BAW0033 sensors. The rotating frequency of the BB units and the rotor was measured with hall sensors (Allegro ATS667LSG). PT100 probes measured the temperature at the

BB outer rings and two pyrometers (Optris CT 3ML) detected the rotor disc temperatures in the BB interfaces. Additionally, two piezoelectric force transducers (PCB 211B with charge amplifier Kistler ICAM 5073A) measured the reaction forces of one BB unit in each plane in the radial direction.

PCI data-acquisition cards (National Instruments) acquired the analog voltage and frequency data produced by the sensors. The position and force signals were acquired at a sample rate of 8 kHz. For the temperatures, a sample rate of 100 Hz was used.

B. Analysis methods

During the delevitation tests thermal, force and position data were acquired and assessed with the following methods.

The position data was processed by the methodology introduced by [12] in order to investigate the severity of different delevitation events. As significant indicators for the severity, the maximum translational speed, and the length of the trajectory of the rotor during the delevitation events were considered.

In Equations 1 and 2, x_i and y_i represent the orthogonal position data of the rotor during the sample number i at the time step t_i of i_{max}measured time steps.

$$v_{max} = \max_{0 \le i \le i_{max}} \frac{\sqrt{(x_i - x_{i-1})^2 + (y_i - y_{i-1})^2}}{t_i - t_{i-1}} \qquad (1)$$

$$d = \sum_{i=1}^{i_{max}} \sqrt{(x_i - x_{i-1})^2 + (y_i - y_{i-1})^2} \qquad (2)$$

The maximum translation speed of the rotor movement v_{max} suggests that high impact forces may occur and quantifies the potential mechanical severity during a delevitation. The length of the trajectory d corresponds to the amount of movement of the rotor. The more the rotor travels inside the BB, the more harming bearing forces can occur and lead to wear of bearing components or even rotor parts. Additionally, the length of the trajectory during a single delevitation event can be summed up to the cumulative trajectory length d_{cum}, given in Equation 3, which can be considered as an operational lifetime measure of the bearing components during the past n delevitation events.

$$d_{\mathrm{cum}} = \sum_{n=1}^{\mathrm{n}_{max}} \mathrm{d_n} \qquad (3)$$

This method was used by [13] in order to observe the BB degradation during consecutive delevitation experiments.

The detected maximum force during the delevitation F_{max} was used as a severity indicator, since it indicates inadmissible bearing loads and reveals the mechanical harmfulness of a delevitation.

The increase of the temperatures of the BB interface surfaces on the discs were analysed in order to detect inappropriate values. The increased temperature ΔT_{rotor} of the rotor discs during the delevitation indicates additional friction induced by the wear (Equation 4). As a result of higher friction in the BB system, it was assumed that the rotor movement and bearing forces increased leading to a possibility of more harmful mechanical damage.

$$\Delta T \propto friction \propto wear \qquad (4)$$

The averaged deceleration rate $\Delta f_{rotor}/\Delta t$ of the rotor and the BBs is useful for determining the increasing friction. If no additional breaking force is applied, it is assumed that the deceleration rate increases with the increased bearing and sliding friction and can indicate degradation induced by the wear and demand for the BB replacement.

The rotor trajectory was analysed in the frequency domain utilizing the Fast Fourier Transform (FFT) to transform the original time-domain data. FFT is a method originally presented by Cooley and Tukey [14]. Filtering out undesired frequency components in the frequency domain is simply conducted by replacing the complex number representing the amplitude and phase of the component with zero (see, e.g., [15]). Since the rotating frequency of the rotor was available through measurements, the frequency spectra of the trajectory could be calculated as a function of the harmonic components of the rotor revolutions. Consequently, harmonic number 1 corresponds to waveforms occurring once per revolution, 2 to phenomena occurring twice per revolution etc. The rotor trajectory is analysed in the frequency domain by utilizing the rotor radial displacement according to the Equation 5.

$$r_i = \sqrt{x_i^2 + y_i^2} \qquad (5)$$

C. Test procedure

The general behaviour and the wear of the rotor and the BB components were investigated with two test series of 135 and 68 deliberate rotor drops in the PBB between 1 and 20 krpm (16 – 333 Hz).

In the test series, the test rig rotor was levitated in its AMB and accelerated to the desired rotational dropping frequency. At dropping frequency, the AMB and the drive were deactivated. Therefore, the rotor dropped in the PBB and ran down with no electric breaking torque.

The first test series was intended to investigate the general behaviour of the rotor in the PBB, the occurring temperatures and the forces at a wide range of dropping frequencies and to verify the usability of the bearing components for high-speed drop downs. In the first test series, 116 of 135 tests were conducted as partial run-downs with relevitation 10 - 20 seconds after the delevitation, when the fast translational rotor movement had settled and no change of behaviour could be observed.

The second test series was conducted to particularly investigate the lifetime and the real service life of the bearing components. Special interest was focused on the high delevitation frequencies, and the durability of the planetary BB system in long-term usage of KES containing multiple high-speed dropdown events. Therefore all 68 tests were full run-downs resulting in durations up to 415 s.

In both test series, the same type of hybrid spindle bearings were used in the backup bearing units. The lubrication of the bearings during the first series was MoS_2, which was applied in a liquid solvent. In the second test series, a special vacuum grease was applied to the bearings by the manufacturer (GMN).

The first test series was continued without a fatal bearing failure. It was finished after a loosened rotor bolt increased the rotor runout significantly. The second test series ended after the metallic debris prevented the appropriate functioning of the AMBs and the electric machine. During the disassembly, one of the BBUs was discovered to have failed.

III. RESULTS

A. General behaviour

The general behaviour of the rotor being dropped on the BB is presented in Figure 4. It shows the trajectory of the rotor in the upper BB plane during a full run-down delevitation event at 20 krpm during the first test series. The first 0.4 s of the run-down is marked in yellow, the following 57 s in blue, and the final phase in orange. The corresponding rotational frequencies of the BBUs and the rotor are displayed in Figure 5. Above 10 krpm, the rotor jumped in a chaotic manner through the polygon shaped free space and had no continuous contact to the BB. Between 10 krpm and 6 krpm the movement of the rotor settled and had short phases of continuous contact in the corners of the BB. Below 6 krpm the rotor stopped moving around and rested in a stable position. The whole run-down took 130 s. The rotational speeds of the six BBUs in the upper PBB plane show that the main synchronization took approximately three seconds. Because of the lack of frictional force from the rotor contact, some BBUs required more time to reach the surface speed of the rotor. Being nearly synchronized and having intermittent contact, the BBUs decelerated together with the rotor. When the jumping movement of the rotor settled, the non-contacted BBUs coasted faster down than the rotor and the contacted BBUs.

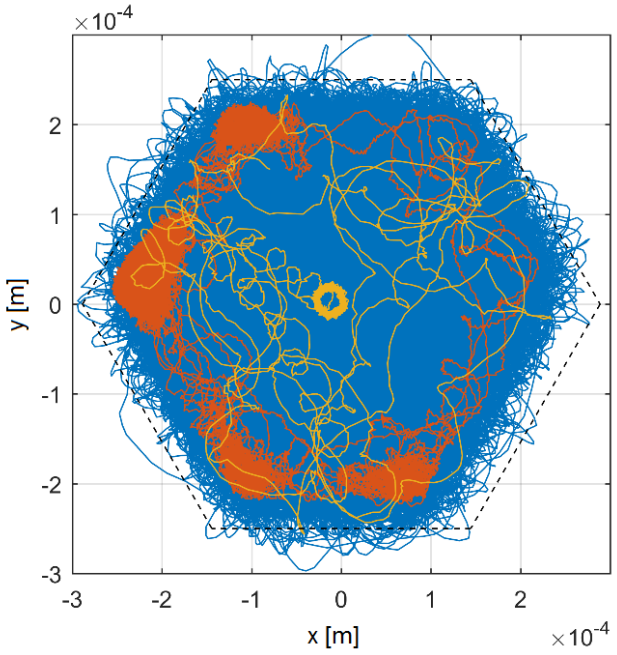

Figure 4. Rotor trajectory in BB plane. Starting phase of the dropping event (yellow), chaotic jumping phase (blue), low activity phase (orange).

The frequency domain spectrum of the rotor movement on the BB plane is presented in Figure 6. The colours on the rotor frequency axis correspond to the colours in Figure 4. Before the dropdown (yellow), all the amplitudes were very low. Small peaks were detected for example in the 1st harmonic component due to unbalance. After dropdown, most of the chaotic jumping movement activity was observed below the 1st harmonic (blue). The transition to the low activity phase (orange) is clearly visible in the spectrum. Moreover, an amplitude peak close to 1st harmonic frequency is clearly observable during the rest of the deceleration.

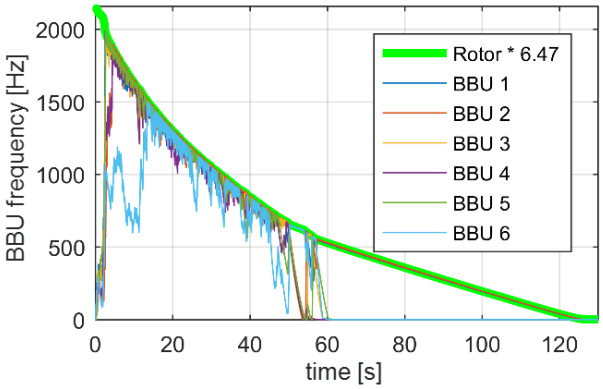

Figure 5. Rotational frequencies of the rotor and six BBUs in the upper plane. Rotor frequency was scaled due to the different diameters.

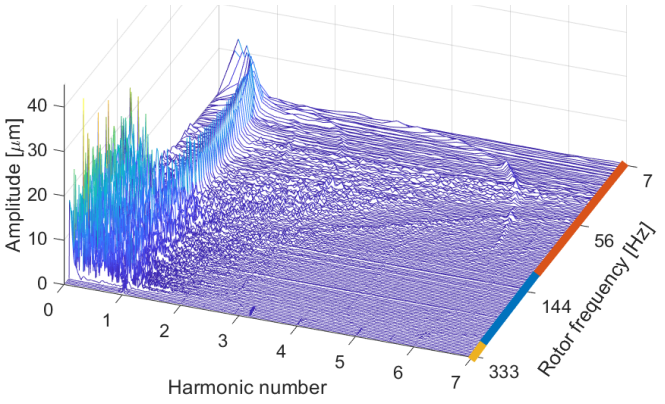

Figure 6. The spectrum presents the trajectory movement amplitudes decomposed to the harmonic components. Harmonic number 1 corresponds to waveforms occurring once per revolution, 2 to phenomena occurring twice per revolution etc. The colours on the rotor frequency axis correspond to the colours in Figure 4.

B. First test series

The first test series showed a significant dependence of severity indicators on the dropping frequency and a trend towards rising severity indicators during consecutive tests.

Figure 7 illustrates the representative data of the first test series. The rotational frequency f_{drop} represents the rotor delevitation frequencies, the length of the trajectory of the rotor restricted by the PBB is represented by d, and the measured maximum bearing force by F_{max}. The partial run-downs are marked with circles while the full run-downs are tagged with crosses. The full run-down presented in Figures 4, 5 and 6 is the only full run-down at 20 krpm (333 Hz) during the first test series.

The MoS_2 lubrication method resulted in a very low lifetime of the lubrication. During the first five drops, the bearing friction rose by the factor of ten, which indicated that the lubrication was worn. The rise of the friction could be determined from the partial run-down tests after the relevitation of the rotor, when the BBUs were decelerated mainly by the friction generated from their axial preload.

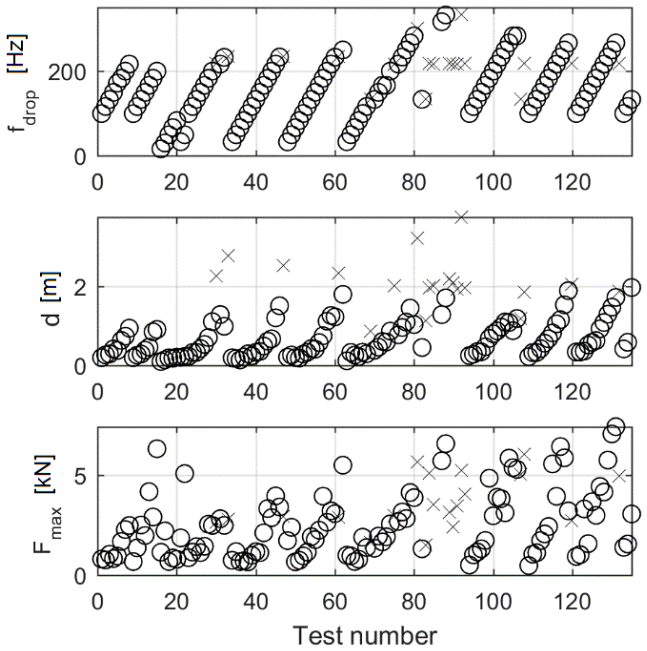

Figure 7. First test series with 19 full run-down tests (crosses) and 115 partial run-downs (circle) in the PBB.

Figure 7 shows that the length of the rotor trajectory restricted by the PBB increased with the growing dropping frequency, and that the obviously longer duration of the full run-downs led clearly to longer trajectory. The highest full run-down delevitation frequency of 333 Hz resulted in a trajectory length of 3.75 m. The sum of the trajectory lengths d_{cum} arrived finally to a length of 114 m after the test series.

The measured maximum force F_{max} also increased with the f_{drop}, but resulted in more random distribution than d, especially in the second half of the test series. Since the friction and force intense phase during the initial synchronization of the BBUs after the drop-down was covered in all the tests, the full run-downs did not show peculiarly higher values in F_{max}. The maximum measured force was 8.31 kN, being nearly double the static load capacity of the bearing pair. Because the measured impact forces lasted only few milliseconds, no remarkable plastic deformation of the bearing races was assumed to occur during these multiple overload situations and the test series could be continued.

Figure 8 presents the dependence of F_{max} and v_{max} on the dropping frequency. With rising dropping frequency, higher severity indicator values could be found in addition to higher variation of the values.

In order to investigate the influence of the increasing wear on severity, test results at the dropping frequency of 217 Hz (13 krpm) were further investigated. The particular dropping frequency was chosen for analysis, because most of the tests were conducted at this frequency. Figure 9 presents the measured maximum forces at a single BBU and the maximum translational speed of the rotor in the upper sensor plane over the cumulated trajectory length of the past tests. It can be seen that both indicators had a trend towards higher severity during the test series. Furthermore, both indicators correlated substantially with each other.

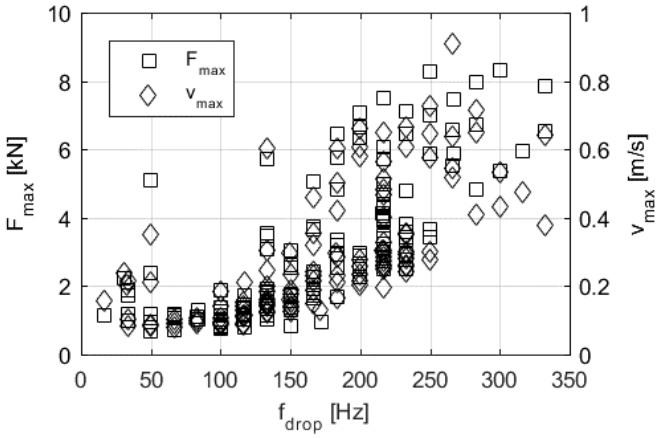

Figure 8. Maximum values of the measured bearing forces and translational rotor speed over the dropping frequency during the first test series.

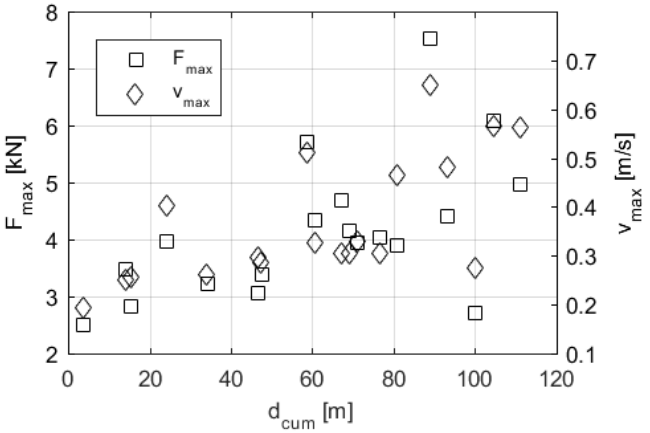

Figure 9. Maximum values of BBU force and translational rotor velocity in the PBB during the first test series delevitations at 217 Hz.

In order to illustrate the wear induced rise of friction in the BB system during the 217 Hz delevitations, the increase of the surface temperature of the rotor is given in Figure 10 and plotted over d_{cum}. The maximum values were measured during the initial synchronization of the BBUs. After the synchronization, the temperatures dropped nearly as fast as they rose within few seconds. A clear trend towards rising temperatures over the test series was detectable, clearly indicating a rising friction, especially after the cumulated trajectory length of 80 m was reached after the 101th test.

After the test series, the visual and manual inspection of the bearing parts showed significant wear of the unhardened rollers and the bearings. Metallic wear debris could be found in the area of the PBB and melted and rolled on the hardened surface of rotor BB interface discs. After cleaning the debris with pressurized air, most of the bearings seemed to be still in relatively good working condition. Plastic deformation in the raceways of some bearings could be found during a microscopic inspection.

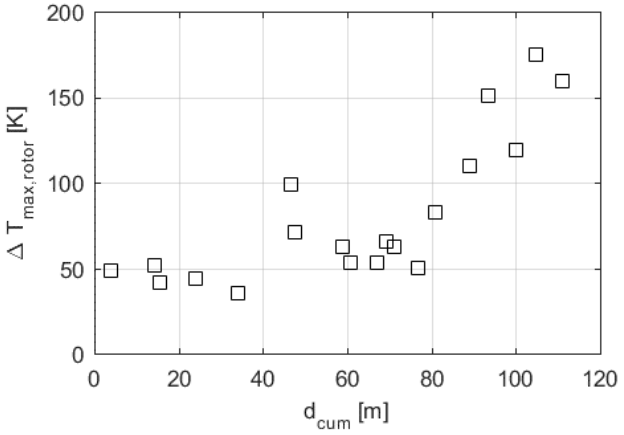

Figure 10. Maximum temperature rise of the BB interface on the rotor discs during the first test series delevitations at 217 Hz.

C. Second test series

The second test series consisted of 68 full run-downs which finally led to a bearing failure. The metallic debris collected to the sensors finally prevented the reliable measurement of the 4 last tests and thus the 64 first tests are presented.

The improved lubrication and lowered preload in the second test series led to much longer run-down times as a result of the lowered system friction. The absolute maximum run-down time of 415 s was measured in the 6th test at a dropping frequency of 267 Hz (16 krpm). During the first test series a maximum run-down time of 131 seconds was measured at a dropping frequency of 333 Hz in the 91th test.

In Figure 11, d and F_{max} are plotted over the test number. After a run-in phase over the first eight tests, the rotor trajectory length remained stable, while the measured forces rose up to 12.5 kN during the 35th test. Further tests showed a trend towards lowering maximum forces. Despite the observed high forces and the remarkably long run-down times due to the full run-downs, a cumulated trajectory length of only 221 m could be achieved, compared to 114 m in the first test series.

In order to investigate further the ongoing wear processes, the severity indicators F_{max}, v_{max} and ΔT_{rotor} of the tests at 217 Hz (13 krpm) were plotted against d_{cum} in Figure 12 and Figure 13. Both F_{max} and v_{max} showed a rising trend up to the middle of the test series at around 125 m in the 35th test. However, the following tests demonstrated a lowering trend. Consistently with the first test series, F_{max} and v_{max} had again a high correlation between each other.

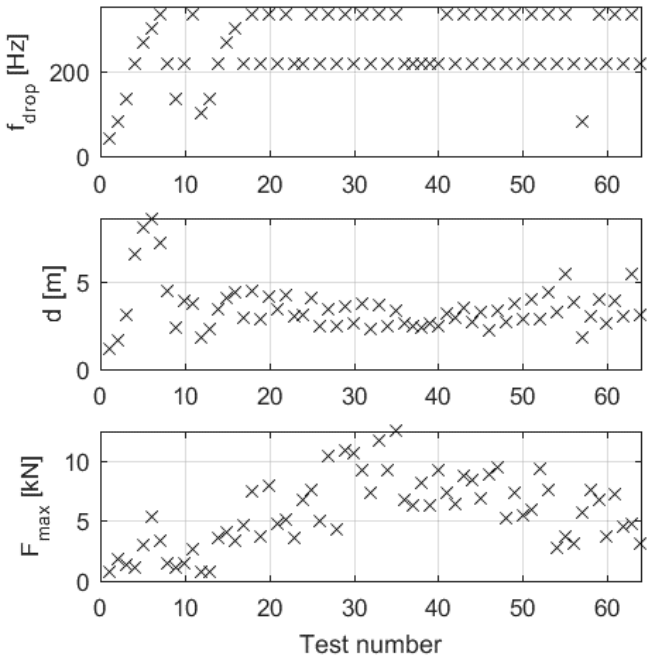

Figure 11. Second test series with 64 full run-down tests (crosses) in the PBB

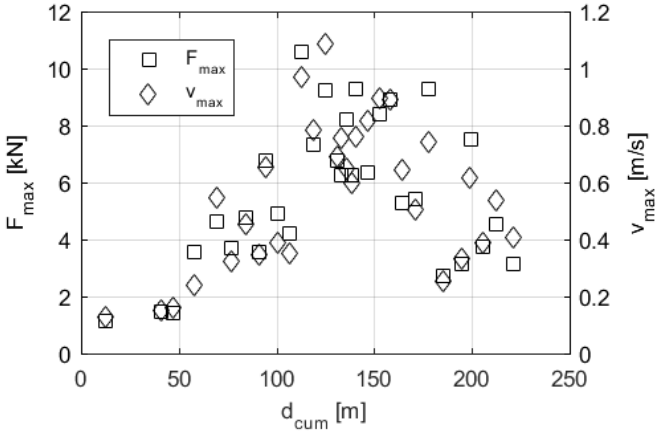

Figure 12. Maximum values of force and translational rotor velocity in the PBB during dropping tests at 217 Hz of the second test series.

The temperature rise of the rotor BB interfaces during the synchronisation showed a different development compared to the previously presented indicators during the test series, which can be seen in Figure 13. Until a cumulated trajectory length of 85 m after the 21th test, the slightly downward trend indicated comparably low frictional energy dissipation in the contact zone. The level was found even lower that in the first test series. Afterwards a significant rising trend was observed and the short term absolute temperature increases of 130 K or more are measured after a trajectory length of 171 m is reached in the 50th test.

The increasing average deceleration rates of the rotor during the run-down indicated also growing friction in the PBB during the test series. To illustrate this, Figure 14 presents the averaged deceleration of the rotor over d_{cum}. Dissimilar to the maximum values of force, speed and temperature rise, the most significant change occurred comparably late after a cumulated trajectory length of 185 m in the 53rd test. Therefore, the average deceleration is a comparably insensitive indicator of short term heavy

BB loads, but clearly shows when the fatal bearing failure is imminent - even when the other indicators no longer seem to be that sensitive.

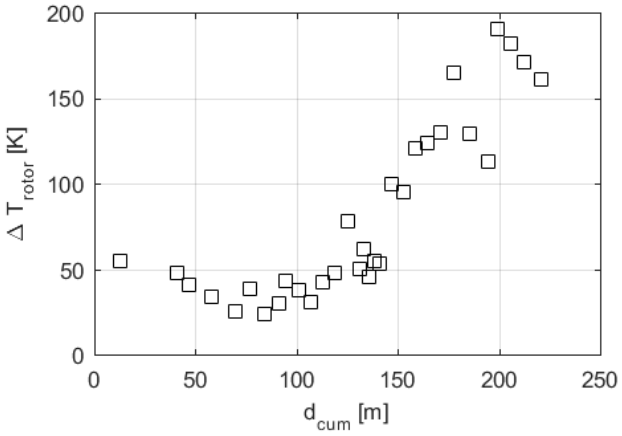

Figure 13. Maximum temperature rise of the BB interface on the rotor during dropping tests at 217 Hz of the second test series.

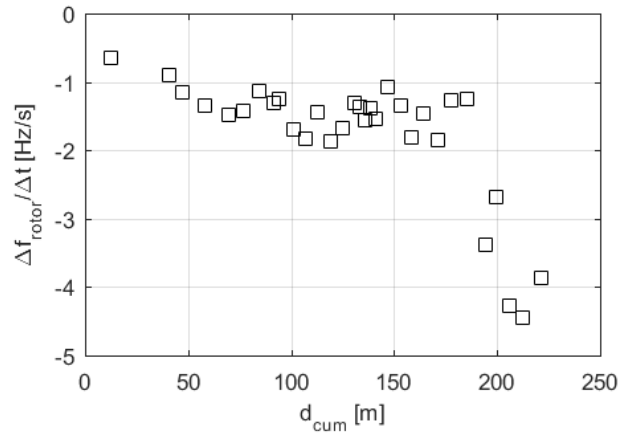

Figure 14. Averaged deceleration of the rotor during dropping tests at 217 Hz of the second test series.

Figures 15, 16 and 17 present the frequency spectra of the rotor radial movement in the upper backup bearing plane during the second test series 20 krpm run-downs number 7, 45 and 53. Lower plane presented similar kind of behaviour. In the 7th test, an obvious transition from the chaotic movement phase to the stabilised movement phase was observed at circa 100 Hz. In the stabilised phase, the spectrum is dominated by the 1st harmonic component due to the unbalance in addition to some low amplitude components at low harmonic frequencies. Generally, most of the frequency domain phenomena occurred in the harmonic component range from 0 to 1, i.e., at a lower frequency than the rotating frequency of the rotor.

The harmonic spectrum calculated from the position data of the 45th test did not produce a similar clear transition towards the stabilised movement phase. The final stabilisation was observed at a frequency of circa 30 Hz. Overall, the spectrum showed a noisier behaviour, and dissimilar to the 7th test, remarkable amplitudes were observable at frequencies higher than the rotating frequency as well.

Finally, the 53rd test at 333 Hz showed chaotic behaviour of the rotor radial movement throughout the deceleration. The amount of vibration at frequencies higher than the rotor frequency increased substantially with the decreasing rotor angular velocity.

Compared to the spectrum of the first test series (Figure 6), the frequency components of the rotor movement in the 7th and the 45th test were much more concentrated in the lower frequency range close to 0th harmonic.

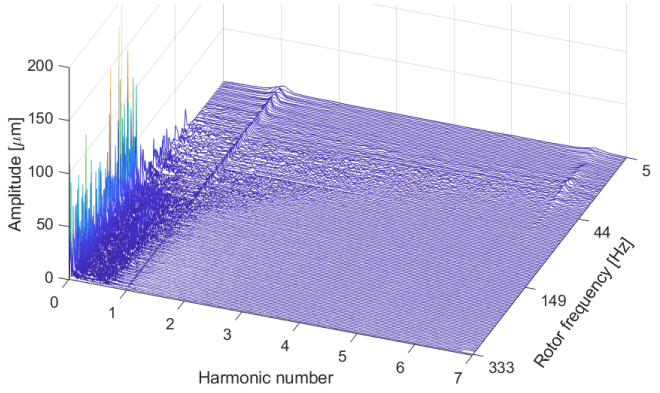

Figure 15. The spectrum of the radial trajectory movement in the 7th test at 333 Hz (20 krpm). A clear transition from the chaotic phase to the stabilised phase at circa 100 Hz was observed.

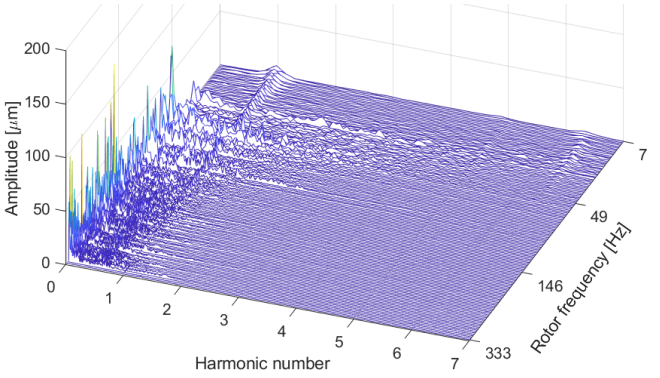

Figure 16. The spectrum of the radial trajectory movement in the 45th test at 333 Hz (20 krpm). The transition to the stabilised movement phase occurred substantially late.

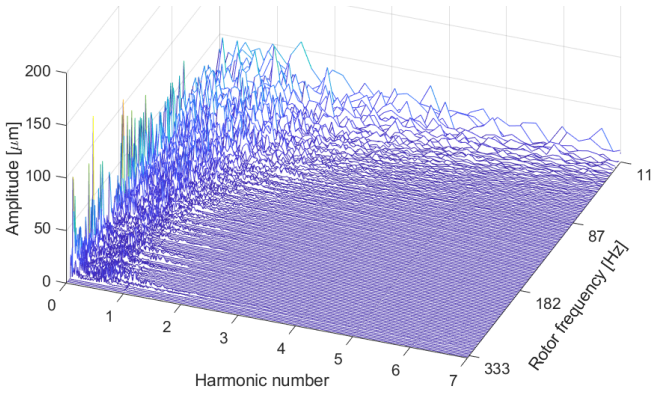

Figure 17. The spectrum of the radial trajectory movement in the 53rd test at 333 Hz (20 krpm). A stabilised movement phase was no more observable.

Figures 18 and 19 present the rotational frequencies of the rotor and the BBUs in the beginning (7th) and in the end (62nd) of the

test series. The 7th test showed a low friction deceleration of the rotor during 330 seconds, including a fast initial synchronisation of the BBUs and finally the low activity phase, which was observed to start after 200 s at the latest.

The 62nd test indicated a clearly elevated friction in the system. The run-down lasted only 50 seconds, and two of the BBUs had constant issues with the synchronisation, even though no low activity phase was observed.

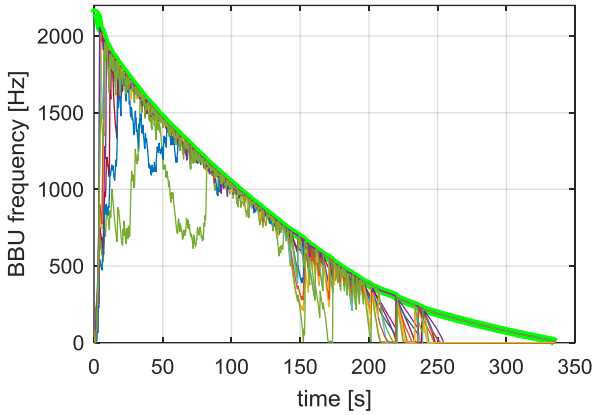

Figure 18. Rotational frequencies of the rotor and both upper and lower plane BBUs in the 7th test at 333 Hz (20 krpm). Rotor frequency was scaled due to the different diameters.

Finally, the second test series was discontinued after 68 tests, because the metallic debris from the rollers and the bearings prevented the appropriate levitation and acceleration of the rotor. The test rig was disassembled, and only then the failure of one BBU was discovered. Figures 20 and 21 present the failed bearing unit after the second test series and a functional bearing unit after the first series. The failed BBU was not able to rotate, some of the ceramic rolling elements were broken and plastic deformation was clearly observable in the bearing components. Metallic debris was rolled and adhered on the outer ring roller element path. Remarkably, all the other BBUs were still able to rotate after the second test series, and after cleaning the debris with pressurized air from the bearings, the functionality improved. The functional BBU after the first series showed plastic deformation and wear as well, but consequently not as extensive as the failed unit.

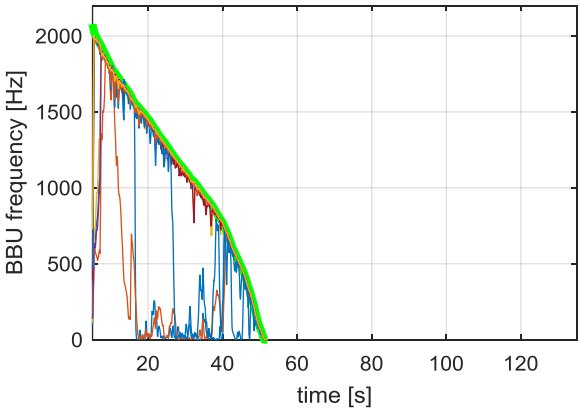

Figure 19. Rotational frequencies of the rotor and both upper and lower plane BBUs in the 62nd test at 333 Hz (20 krpm). Rotor frequency was scaled due to the different diameters.

Figure 20. Bearing inner rings and BBU rollers. Left: the failed backup bearing components after the second test series. Right: functional components after the first test series.

Figure 21. Bearing outer rings and ceramic balls. Left: the failed backup bearing components from the second test series. Right: functional components from the first test series.

IV. Discussion

The results suggest that the planetary backup bearing approach is valid and utilizable in the present application. Partly caused by the design principle, heavy impacts are caused during the synchronisation phase, which imposes boundary conditions to the bearing selection.

The severity indicators analysed in the present study quantified the harshness of the drop-downs. They can be used in assessing the intensity of the past dropping events in addition to determining the backup bearing life if enough experimental data is available. The typically available measurements such as rotor position and the rotor speed provide a good opportunity for the life time estimation as well, considering the maximum translational velocity and deceleration rate of the rotor frequency after the delevitation.

The decreased pretension and the vacuum suitable grease of the bearings was found to decrease the friction of the backup bearings judging by the substantially increased run-down times of the delevitated rotor. Consequently, the increased run-down times were observable only in the beginning of the second test series, since the wear substantially increased the deceleration rate with the advancing number of delevitations.

The frequency domain spectra depicting the planetary backup bearing in the second test series showed the backup bearing condition in three different stages. The 7th test showed a fully functional backup bearing with minimal wear and a clear transition to the stabilised movement phase. The 45th test showed the behaviour after a considerable number of high-speed full run-downs. The wear in the BBU components can be seen as a later transition to the low activity phase and a generally noisier behaviour. Finally, the 53rd test showed the behaviour, when the bearings were assumed to be approaching the end of their life-time. Compared to the first test series, the concentration of the frequency components closer to the 0th har-

monic in the second test series suggests, that the rotor translational movement showed lower frequency behaviour possibly leading to lower forces and declined wear.

The second test series was not discontinued due to a critical damage of the rotor, electric motor or the AMBs, but the amount of metallic debris in the functional parts of the system. The planetary backup bearing was found to be able to sustain the rotor during the run-down by the 11 functional BBUs, although one of the BBUs was completely failed. This feature is seen highly valuable considering the fail-safety of the planetary backup bearing and kinetic energy storages in general.

V. Conclusion

The experimental testing of the gyroscopic and rigid rotor supported by a planetary backup bearing (PBB) after a delevitation showed promising results considering the general behaviour and lifetime expectations. The obtained results suggest that the occurring forces and temperatures are at a manageable level for the rotor and stator components, even in a vacuum environment. Because critical speeds of the rotor were not passed during the experiments, the synchronisation was identified as the most harmful phase of the run-down with highest thermal and mechanical loads. At medium rotational speeds, the rotor was stabilised in the corners of the polygon shaped PBB producing the lowest loads, which is a desirable state for the whole run-down. Consequently, the stabilisation became more unlikely with the increasing number of tests indicating wear in the PBB. The stabilisation in the corners should be investigated and provoked with special mechanisms or properties of the BBUs in the future work. For example, an asymmetric shape of the PBB polygon or varying stiffness and damping properties of the BBUs could be investigated.

The used severity indicators were found useful to enable the observation of advancing wear and to quantify and summarize the severity of the past rotor drops. The cumulated trajectory length was found to be a useful method to quantify the past run-downs and to estimate the remaining service life of the BB system. The utilisation of the maximum values of translational velocity and force during single dropping tests quantified well the mechanical harmfulness of a delevitation. Since the maximum velocity and force correlated relatively well, the complex and expensive force measurement can be omitted in an industrial application. The observation of the temperature rises of the BB components gave the opportunity to quantify the increased friction and wear caused by the past delevitations. Together with the averaged deceleration of the rotor, heavy advancing bearing degradation could be observed before fatal bearing failure took place.

Regarding the application of the planetary backup bearing in a kinetic energy storage of outer rotor type, multiple high-speed drop-downs with following run-downs are assumed to be possible without a significant increase of delevitation severity. To extend the lifetime of the PBB, the most achievable manners are active emergency braking and fast relevitation of the rotor. Additionally, special surface treatment such as hardening of the rollers and robust coatings of the bearing components may also extend the lifetime and probably lead to lower severity.

Considering that the test rig rotor is much lighter than the ORT flywheels, the bearings of the PBB should have a higher load rating, although multiple short overloads showed no fatal damage during the two test series. This could ensure a longer lifetime and less harmful delevitations. An experimental investigation of a full-size kinetic energy storage should be a next step in order to verify the planetary backup bearing for commercial applications. Preliminary simulation investigations suggest that the decreased number of the backup bearing units can positively influence delevitation severity, which should also be investigated experimentally.

Acknowledgments

This research work was supported by Federal Ministry for Economic Affairs and Energy on the basis of a decision by the German Bundestag. In addition, the work was supported by Academy of Finland (project TwinRotor).

References

[1] J. VanderMeer, M. Mueller-Stoffels, and E. Whitney “An Alaska case study: Energy storage technologies,” *Journal of Renewable and Sustainable Energy*, vol 9, 061708, 2017.

[2] T. Bocklisch, “Hybrid energy storage systems for renewable energy applications,” *Energy Procedia*, vol. 73, pp. 103-111, 2015.

[3] M. Hedlund, J. Lundin, J. de Santiago, J. Abrahamsson and Hans Bernhoff, “Flywheel Energy Storage for Automotive Applications,” *Energies*, vol. 8, pp. 10636-10663, 2015.

[4] U. of Sheffield, “Europe’s largest hybrid flywheel battery project to help grid respond to energy demand“, 02-July-2017. Retrieved online from https://www.sheffield.ac.uk/news/nr/flywheel-europe-energy-1.704921 on 27-June-2018.

[5] Hawkins, L., McMullen, P. and Larsonneur, R., “Development of an AMB Energy Storage Flywheel for Commercial Applications,” *Proc. 8th International Symposium on Magnetic Suspension Technology*, Dresden, Germany, 2005.

[6] P. McMullen, L. Hawkins, “Long Term Backup Bearing Testing Results,” *13th International Symposium on Magnetic Bearings*, Arlington, USA, 2012.

[7] L. Quurck, M. Richter, M. Schneider, D. Franz, S. Rinderknecht, “Design and practical realization of an innovative flywheel concept for industrial applications,” *Technische Mechanik* vol. 37, Issue 2-5 pp. 151-160, 2017.

[8] L. Quurck, H. Schaede, M. Richter, S. Rinderknecht, “High Speed Backup Bearings for Outer-Rotor-Type Flywheels - Proposed Testrig Design,” *Proceedings of ISMB14*, Linz, Austria, 2014.

[9] L. Quurck, D. Franz, B. Schüßler, S. Rinderknecht, “Planetary backup bearings for high speed applications and service life estimation methodology,” *Mechanical Engineering Journal*, vol. 4, Issue 5, 2017.

[10] H. Ming Chen, J. Walton, H. Heslunat, “Zero Clearance Auxiliary Bearings for Magnetic Bearing Systems,” *International Gas Turbine & Aeroengine Congress & Exhibition*, Orlando, USA, 1997.

[11] G. Schubert, H. Walter, “Fanglager zum Auffangen einer Rotorwelle einer Maschine”, Patent, DE102009031887 A1, 2011.

[12] J. J. Janse van Rensburg, G.V. Schoor, P.V. Vuuren, “The characterization of the severity of rotor delevitation events: A parametric study,” *Proceedings of ISMB13*, Arlington, 2012.

[13] Gouws, J.M. and Rensburg, J.J.V. “An Investigation into Backup Bearing Life using Quantified Rotor Delevitation Severity Indicators,” *Proceedings of ISMB15*, Kitakyushu, Japan, 2016.

[14] J.W. Cooley, J.W. Tukey, “An algorithm for the machine calculation of complex Fourier series,” *Mathematics of computation* vol. 19, pp. 297–301, 1965.

[15] P.A. Mosier-Boss, S.H. Lieberman, R. Newbery, “Fluorescence rejection in Raman spectroscopy by shifted-spectra, edge detection, and FFT filtering techniques,” *Applied Spectroscopy* vol. 49, pp. 630–638, 1995.